Supplementary Information

# Pitfalls in Probing Hydroxyl Radical by Electron Paramagnetic Resonance Spectroscopy in Persulfate-based Systems

Zhen Qi[a], Zhuning Geng[a], Fangzhou Li[a], Di Zheng[a], Guanghe Li[a], Fang Zhang[a,b*]

[a] School of Environment, State Key Laboratory of Regional Environment and Sustainability, Tsinghua University, Beijing, 100084, PR China

[b] National Engineering Laboratory for Site Remediation Technologies (NEL-SRT), Beijing 100015, China

# Supplementary Information

## Table of Contents

Table S1. Electrostatic potential (ESP) surface analysis summary of DMPO/$SO_4^{\bullet-}$ and $SO_4^{\bullet-}$ 4

Table S2. Contributions to LUMO orbitals by individual atoms of DMPO/$SO_4^{\bullet-}$ and $SO_4^{\bullet-}$ ... 4

Table S3. Reaction network for the kinetic model with DMSO..... 5

Table S4. Reaction network for the kinetic model without DMPO and DMSO ..... 5

Table S5. The second-order rate constants for the reaction of $SO_4^{\bullet-}$ and •OH with common compounds used in this study..... 6

Figure S1. Surface area in specific value range of ESP mapped function of $SO_4^{\bullet-}$..... 6

Figure S2. Surface area in specific value range of ESP mapped function of DMPO/$SO_4^{\bullet-}$..... 7

Figure S3. The contribution of different nucleophiles ($H_2O$ and $OH^-$) for the hydrolysis of $SO_4^{\bullet-}$.. ..... 7

Figure S4. The contribution of different nucleophiles ($H_2O$ and $OH^-$) for the hydrolysis of DMPO/$SO_4^{\bullet-}$..... 8

Figure S5. Schematic representation of the transition states of the $OH^-$ reacting with DMPO/$SO_4^{\bullet-}$ and $SO_4^{\bullet-}$ ..... 8

Figure S6. Fitting of the rate constant of actual concentration of $S_2O_8^{2-}$..... 9

Figure S7. The contribution of different reactions for DMPO/•OH..... 9

Figure S8. The contribution of free •OH pathway and hydrolysis pathway for DMPO/•OH accumulation without DMSO..... 10

Figure S9. The contribution of free •OH pathway and hydrolysis pathway for DMPO/•OH accumulation with DMSO..... 10

Figure S10. The steady-state concentration of $H^+$ under different initial pH (pH = 3, 5, 7, 9, and 11)..... 11

References ..... 12

Table S1. Electrostatic potential (ESP) surface analysis summary of DMPO/$SO_4^{\bullet-}$ and $SO_4^{\bullet-}$

| Species | Surface area /Å² | Average value /kcal/mol | Maximum /kcal/mol | Minimum /kcal/mol | Reaction site /kcal/mol |
|---|---|---|---|---|---|
| $SO_4^{\bullet-}$ | 102.0 | -115.7 | -101.2 | -125.0 | -105.5 |
| DMPO/$SO_4^{\bullet-}$ | 225.0 | -79.7 | -14.7 | -152.2 | -21.3 |

Table S2. Contributions to LUMO orbitals by individual atoms of DMPO/$SO_4^{\bullet-}$ and $SO_4^{\bullet-}$

| Species | NO. | Percent/% | Species | NO. | Percent/% |
|---|---|---|---|---|---|
| DMPO/$SO_4^{\bullet-}$ | 1(N) | 36.96 | $SO_4^{\bullet-}$ | 1(O) | 21.87 |
| | 2(C) | 2.46 | | 2(O) | 21.87 |
| | **3(C)** | **4.42** | | 3(O) | 49.55 |
| | 4(O) | 42.07 | | **4(O)** | **1.39** |
| | 5(C) | 0.51 | | 5(S) | 5.32 |
| | 6(C) | 1.47 | | | |
| | 7(C) | 2.32 | | | |
| | 8(C) | 0.67 | | | |
| | 9(O) | 3.28 | | | |
| | 10(S) | 1.19 | | | |
| | 11(O) | 0.81 | | | |
| | 12(O) | 0.40 | | | |
| | 13(O) | 0.53 | | | |
| | 14(H) | 1.13 | | | |
| | 15(H) | 0.04 | | | |
| | 16(H) | 0.12 | | | |
| | 17(H) | 0.07 | | | |
| | 18(H) | 0.26 | | | |
| | 19(H) | 0.06 | | | |
| | 20(H) | 0.06 | | | |
| | 21(H) | 0.11 | | | |
| | 22(H) | 0.47 | | | |
| | 23(H) | 0.31 | | | |
| | 24(H) | 0.29 | | | |
| | 23(H) | 0.31 | | | |
| | 24(H) | 0.29 | | | |

Delocalization index of DMPO/$SO_4^{\bullet-}$ and $SO_4^{\bullet-}$: 31.84 and 34.42.

Table S3. Reaction network for the kinetic model with DMSO

| No. | Reaction | Rate constant | Source |
|---|---|---|---|
| 1 | Fe-pyrite + $S_2O_8^{2-}$ → $SO_4^{\bullet-}$ + $SO_4^{2-}$ | $2.9 \times 10^{-4}$ $M^{-1}$ $s^{-1}$ | this study[a] |
| 2 | $SO_4^{\bullet-}$ + $SO_4^{\bullet-}$ → $S_2O_8^{2-}$ | $4.4 \times 10^{8}$ $M^{-1}$ $s^{-1}$ | (Wei et al. 2017) |
| 3 | $SO_4^{\bullet-}$ + $OH^-$ → $SO_4^{2-}$ + •OH | $6.5 \times 10^{7}$ $M^{-1}$ $s^{-1}$ | (Hayon et al. 1972) |
| 4 | $SO_4^{\bullet-}$ + •OH → $HSO_5^-$ | $1.0 \times 10^{10}$ $M^{-1}$ $s^{-1}$ | (Buxton et al. 1988) |
| 5 | $SO_4^{\bullet-}$ + $H_2O$ → $SO_4^{2-}$ + •OH + $H^+$ | $1.2 \times 10^{1}$ $s^{-1}$ | (NIST 2020) |
| 6 | •OH + $S_2O_8^{2-}$ → $S_2O_8^{\bullet-}$ + $OH^-$ | $1.4 \times 10^{7}$ $M^{-1}$ $s^{-1}$ | (Yang et al. 2014) |
| 7 | $S_2O_8^{2-}$ + $SO_4^{\bullet-}$ → $SO_4^{2-}$ + $S_2O_8^{\bullet-}$ | $6.6 \times 10^{5}$ $M^{-1}$ $s^{-1}$ | (Wei et al. 2017) |
| 8 | DMPO + $SO_4^{\bullet-}$ → DMPO/$SO_4^{\bullet-}$ | $2.9 \times 10^{4}$ $M^{-1}$ $s^{-1}$ | (Wei et al. 2017) |
| 9 | DMPO + •OH → DMPO/•OH | $3.3 \times 10^{9}$ $M^{-1}$ $s^{-1}$ | (Goldstein et al. 2004) |
| 10 | DMPO/$SO_4^{\bullet-}$ + $OH^-$ → DMPO/•OH + $SO_4^{2-}$ | $5.2 \times 10^{8}$ $M^{-1}$ $s^{-1}$ | this study[b] |
| 11 | DMPO/$SO_4^{\bullet-}$ + $H_2O$ → DMPO/•OH + $H^+$ + $SO_4^{2-}$ | $8.9 \times 10^{2}$ $s^{-1}$ | (Wei et al. 2017) |
| 12 | DMPO/•OH → Product1 | $7.0 \times 10^{-3}$ $s^{-1}$ | (Wei et al. 2017) |
| 13 | DMPO/$SO_4^{\bullet-}$ → Product2 | $1.5 \times 10^{-6}$ $s^{-1}$ | (Zalibera et al. 2009) |
| 14 | •OH + $(CH_3)_2SO$ (DMSO) → $(CH_3)SOOH$ + $•CH_3$ | $k = 7 \times 10^{9}$ $M^{-1}$ $s^{-1}$ | (Avraham et al. 2022) |

Table S4. Reaction network for the kinetic model without DMPO and DMSO

| No. | Reaction | Rate constant | Source |
|---|---|---|---|
| 1 | Fe-pyrite + $S_2O_8^{2-}$ → $SO_4^{\bullet-}$ + $SO_4^{2-}$ | $2.9 \times 10^{-4}$ $M^{-1}$ $s^{-1}$ | this study[a] |
| 2 | $SO_4^{\bullet-}$ + $SO_4^{\bullet-}$ → $S_2O_8^{2-}$ | $4.4 \times 10^{8}$ $M^{-1}$ $s^{-1}$ | (Wei et al. 2017) |
| 3 | $SO_4^{\bullet-}$ + $OH^-$ → $SO_4^{2-}$ + •OH | $6.5 \times 10^{7}$ $M^{-1}$ $s^{-1}$ | (Hayon et al. 1972) |
| 4 | $SO_4^{\bullet-}$ + •OH → $HSO_5^-$ | $1.0 \times 10^{10}$ $M^{-1}$ $s^{-1}$ | (Buxton et al. 1988) |
| 5 | $SO_4^{\bullet-}$ + $H_2O$ → $SO_4^{2-}$ + •OH + $H^+$ | $1.2 \times 10^{1}$ $s^{-1}$ | (NIST 2020) |
| 6 | •OH + $S_2O_8^{2-}$ → $S_2O_8^-$ + $OH^-$ | $1.4 \times 10^{7}$ $M^{-1}$ $s^{-1}$ | (Yang et al. 2014) |
| 7 | $S_2O_8^{2-}$ + $SO_4^{\bullet-}$ → $SO_4^{2-}$ + $S_2O_8^{\bullet-}$ | $6.6 \times 10^{5}$ $M^{-1}$ $s^{-1}$ | (Wei et al. 2017) |

Table S5. The second-order rate constants for the reaction of $SO_4^{\bullet-}$ and •OH with common compounds used in this study

| Compound | $k_{SO4\bullet-}$ | $k_{\bullet OH}$ | Source |
|---|---|---|---|
| SIX | $1.60 \times 10^{11}$ | $7.35 \times 10^{9}$ | (Zhang et al. 2016) |
| SMP | $8.1 \times 10^{10}$ | $6.2 \times 10^{9}$ | (Zhang et al. 2016) |
| GEM | $4.78 \times 10^{9}$ | $9.86 \times 10^{9}$ | (Gao et al. 2022, Zhou et al. 2020) |
| ATZ | $3.5 \times 10^{9}$ | $3.0 \times 10^{9}$ | (Acero et al. 2000, Lutze et al. 2015) |
| CAP | $9.1 \times 10^{8}$ | $1.80 \times 10^{9}$ | (Gao et al. 2022, Kapoor and Varshney 1997) |
| PMD | $5.3 \times 10^{8}$ | $6.7 \times 10^{9}$ | (Nihemaiti et al. 2018, Real et al. 2009) |
| PFOA | $2.6 \times 10^{5}$ | $<10^{5}$ | (Mitchell et al. 2014, Qian et al. 2016) |

SIX: sulfisoxazole, SMP: sulfamethoxypyridazine, GEM: gemfibrozil, ATZ: atrazine, CAP: chloramphenicol, PMD: primidone, PFOA: perfluorooctanoic acid ammonium salt.

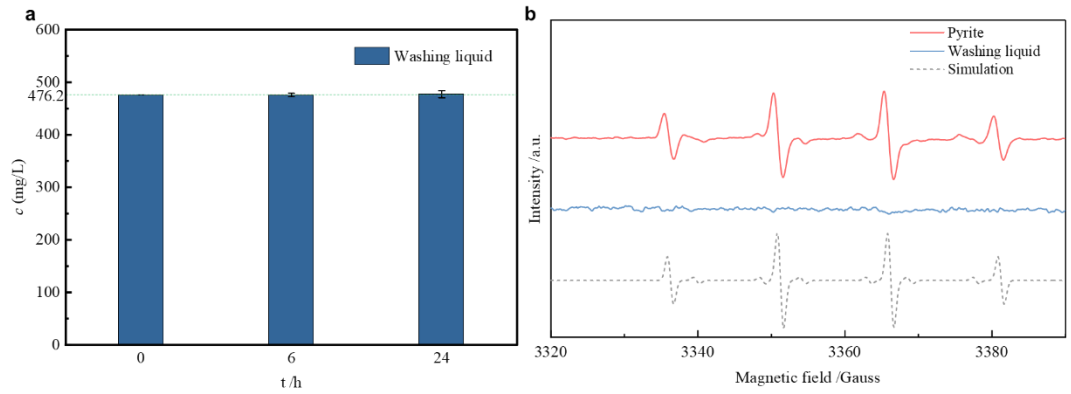


Figure S1. Effect of PDS activated by dissolved iron ion in washing liquid activation before and after reaction. (a) PDS concentration of washing; (b) EPR spectra of adducts with •OH and $SO_4^{\bullet-}$ by DMPO in washing liquid systems. Conditions: [PDS] = 2 mmol/L, $T$ = 25°C, [$FeS_2$] = 100 g/L.

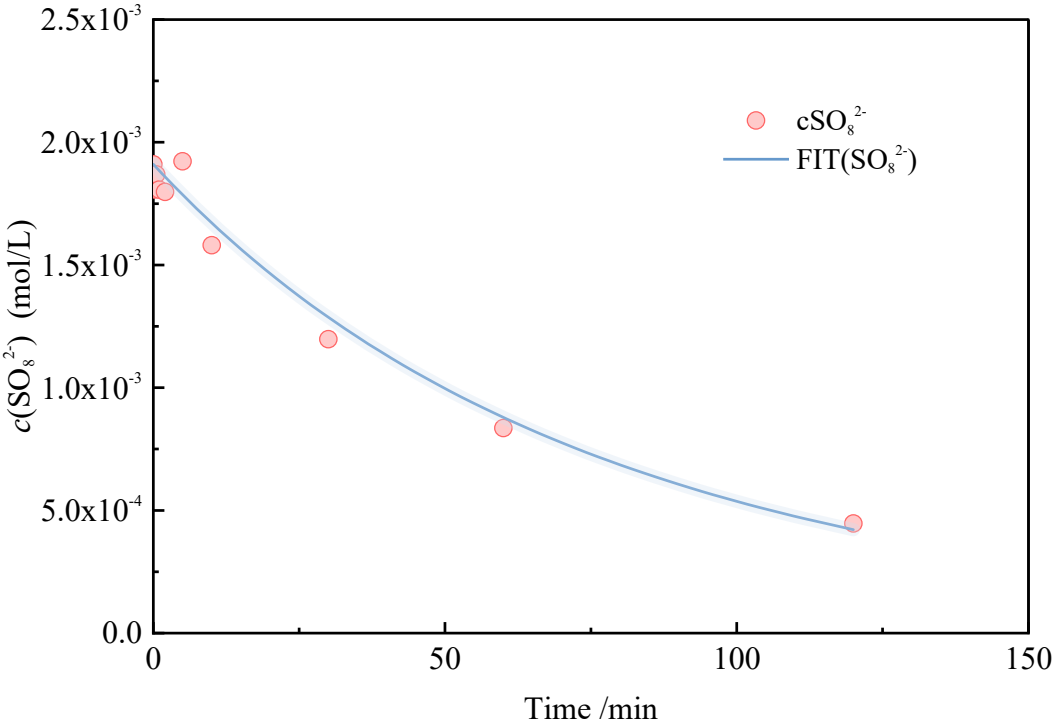


Figure S2. Fitting of the rate constant of the actual concentration of $S_2O_8^{2-}$. [PDS] = 100 mmol/L, $T$ = 25℃, [$FeS_2$] = 100 g/L, pH=3.3.

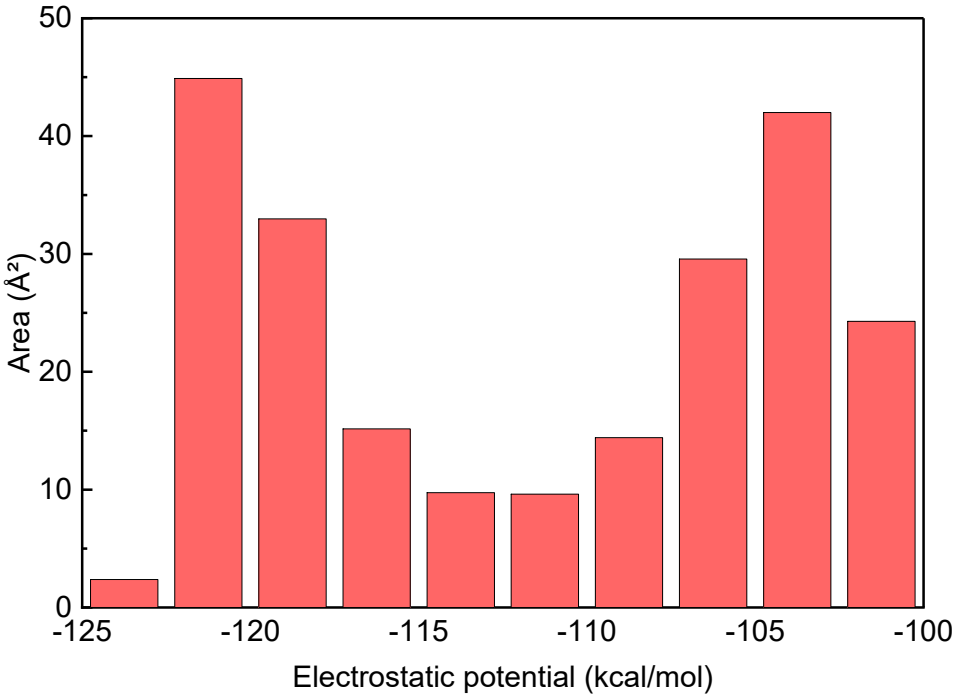


Figure S3. Surface area in a specific value range of the ESP mapped function of $SO_4^{\bullet-}$.

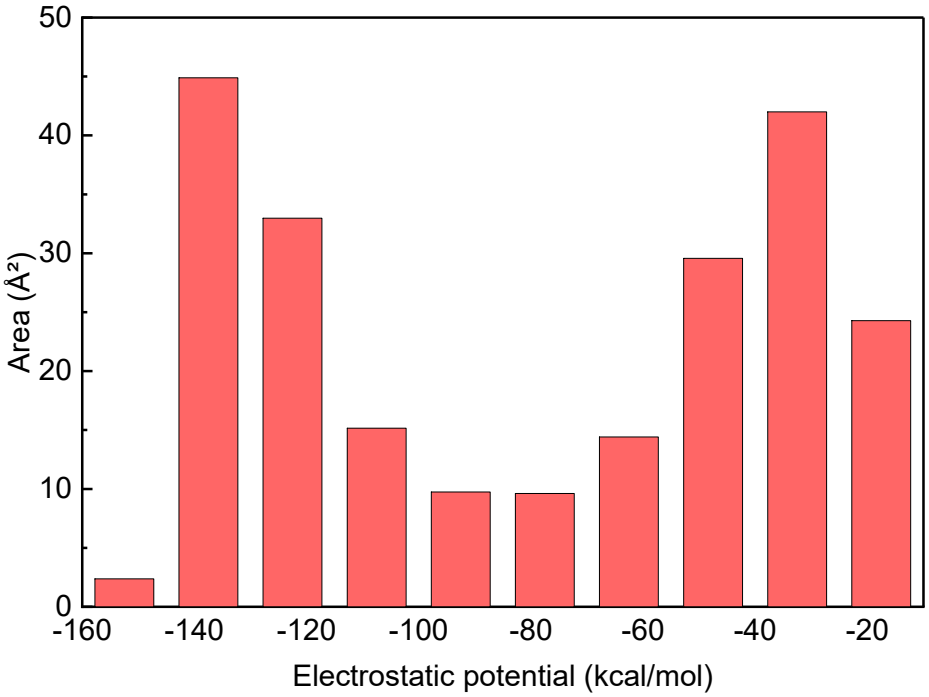


Figure S4. Surface area in a specific value range of the ESP mapped function of DMPO/$SO_4^{\bullet-}$.

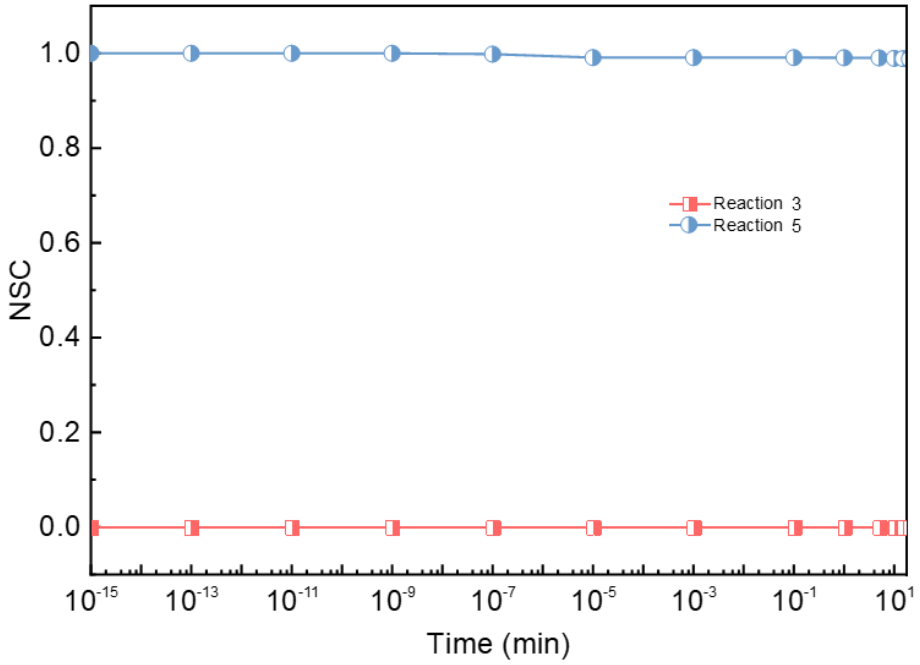


Figure S5. The contribution of different nucleophiles ($H_2O$ and $OH^-$) for the hydrolysis of $SO_4^{\bullet-}$.

Simulation conditions: [$FeS_2$] = 100 g/L, [DMPO] = 110 mmol/L, [Persulfate] = 100 mmol/L, T=25 ℃, pH=3.33.

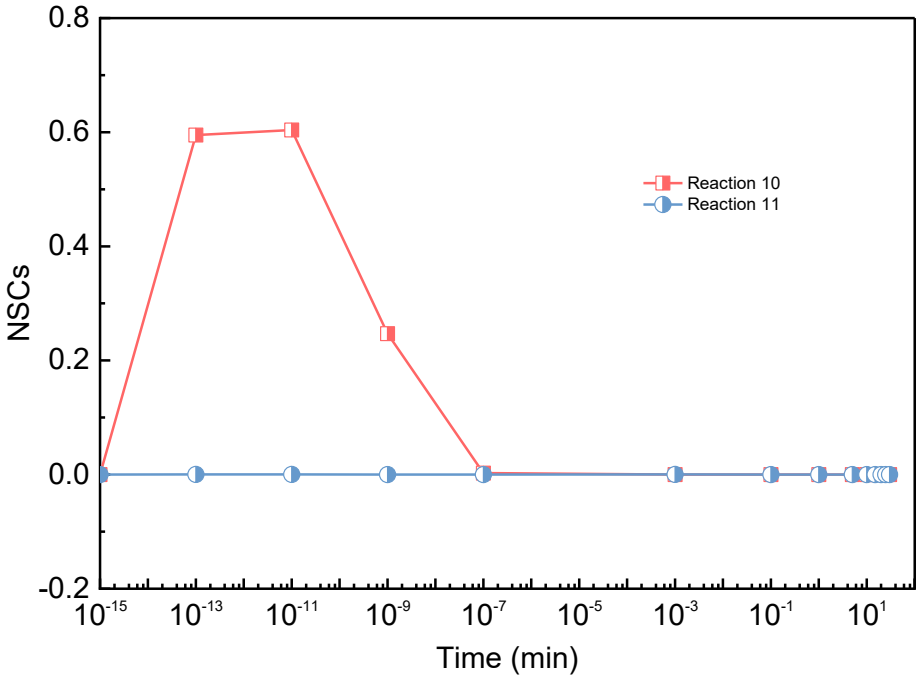


Figure S6. The contribution of different nucleophiles ($H_2O$ and $OH^-$) for the hydrolysis of DMPO/$SO_4^{\bullet-}$. Simulation conditions: [$FeS_2$] = 100 g/L, [DMPO] = 110 mmol/L, [Persulfate] = 100 mmol/L, T=25 ℃, pH=3.33.

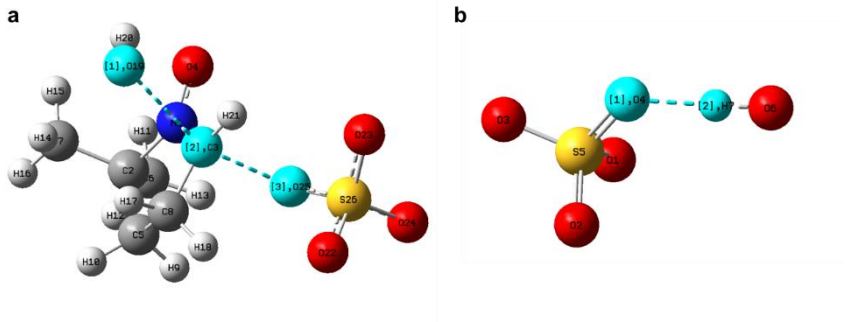


Figure S7. Schematic representation of the transition states of the $OH^-$ reacting with DMPO/$SO_4^{\bullet-}$ and $SO_4^{\bullet-}$.

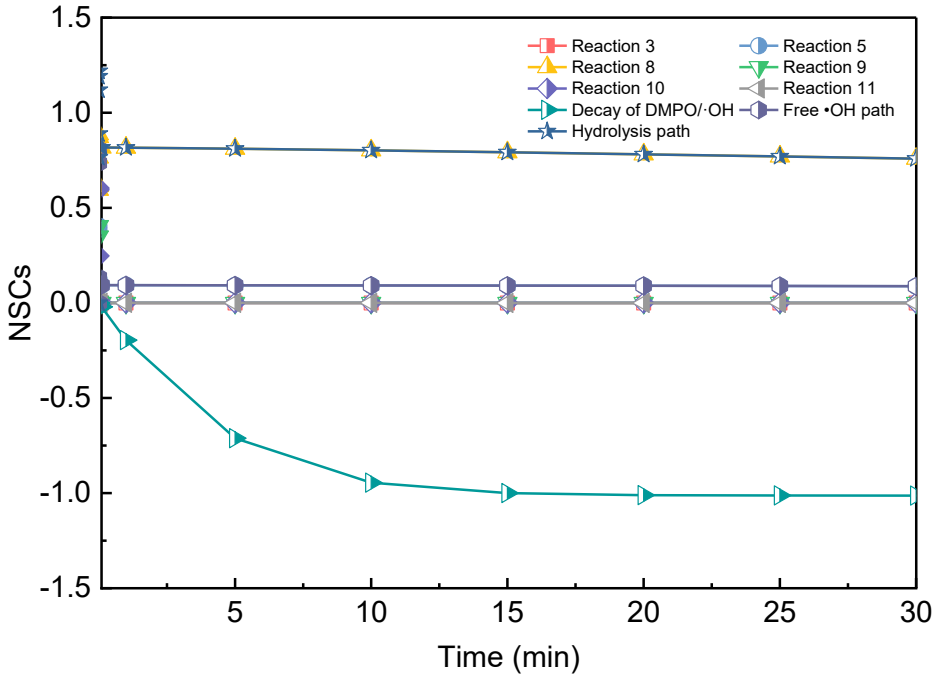


Figure S8. The contribution of different reactions for DMPO/•OH. Simulation conditions: [$FeS_2$] = 100 g/L, [DMPO] = 110 mmol/L, [Persulfate] = 100 mmol/L, T=25 ℃, pH=3.33.

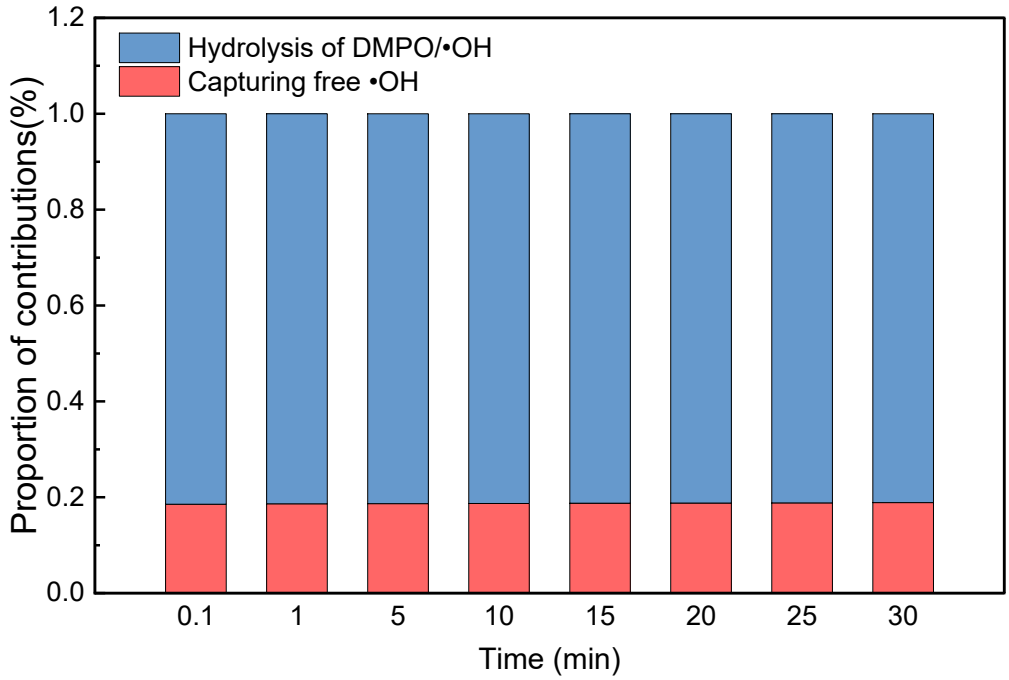


Figure S9. The contribution of the free •OH pathway and hydrolysis pathway for DMPO/•OH accumulation without DMSO.

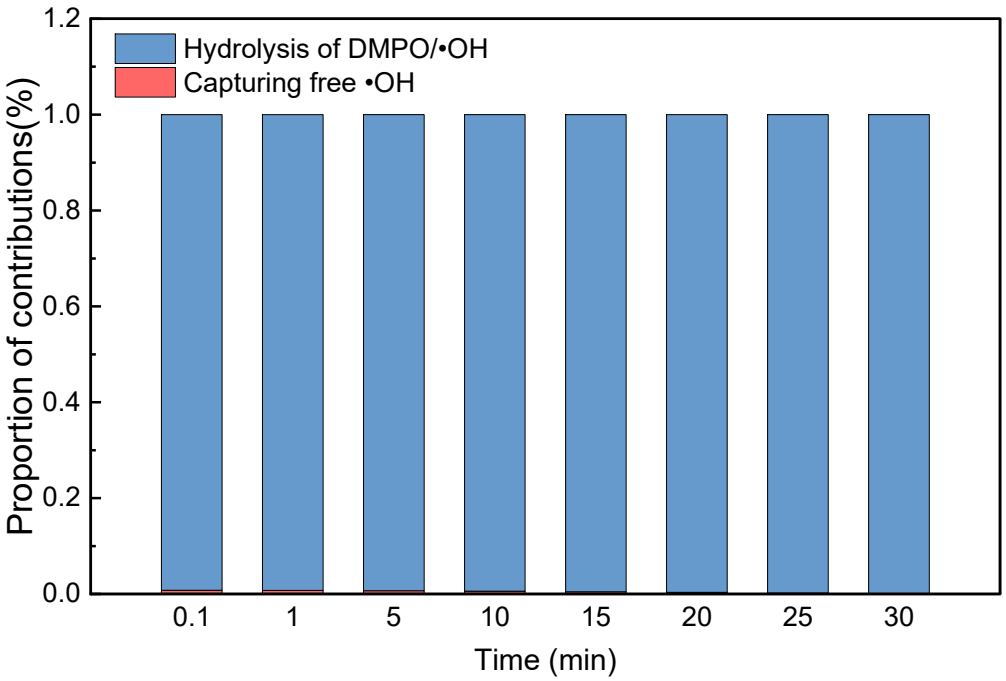


Figure S10. The contribution of the free •OH pathway and hydrolysis pathway for DMPO/•OH accumulation with DMSO.

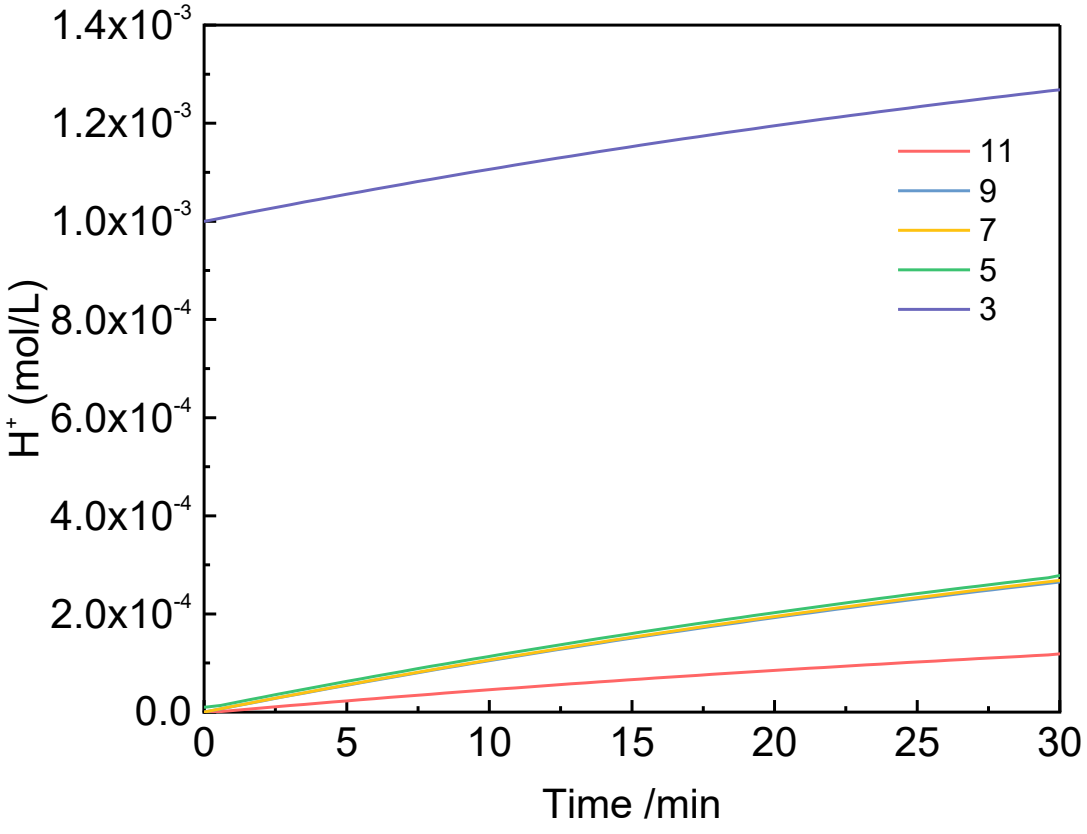

Figure S11. The steady-state concentration of $H^+$ under different initial pH (pH = 3, 5, 7, 9, and 11). Simulation conditions: [$FeS_2$] = 100 g/L, [DMPO] = 110 mmol/L, [Persulfate] = 100 mmol/L, T=25 ℃.

References

Acero, J.L., Stemmler, K. and von Gunten, U. (2000) Degradation Kinetics of Atrazine and Its Degradation Products with Ozone and OH Radicals: A Predictive Tool for Drinking Water Treatment. Environmental Science & Technology 34 (4), 591-597.

Avraham, E., Meyerstein, D., Lerner, A., Yardeni, G., Pevzner, S., Zilbermann, I., et al. (2022) Reactions of methyl, hydroxyl and peroxyl radicals with the DOTA chelating agent used in medical imaging. Free Radical Biology and Medicine 180, 134-142.

Buxton, G.V., Greenstock, C.L., Helman, W.P. and Ross, A.B. (1988) Critical Review of rate constants for reactions of hydrated electrons, hydrogen atoms and hydroxyl radicals (•OH/•$O^-$) in Aqueous Solution. Journal of Physical and Chemical Reference Data 17 (2), 513-886.

Gao, L., Guo, Y., Huang, J., Wang, B., Deng, S., Yu, G., et al. (2022) Simulating micropollutant abatement during cobalt mediated peroxymonosulfate process by probe-based kinetic models. Chemical Engineering Journal 441, 135970.

Goldstein, S., Rosen, G.M., Russo, A. and Samuni, A. (2004) Kinetics of Spin Trapping Superoxide, Hydroxyl, and Aliphatic Radicals by Cyclic Nitrones. The Journal of Physical Chemistry A 108 (32), 6679-6685.

Hayon, E., Treinin, A. and Wilf, J. (1972) Electronic spectra, photochemistry, and autoxidation mechanism of the sulfite-bisulfite-pyrosulfite systems. $SO_2^-$, $SO_3^-$, $SO_4^-$, and $SO_5^-$ radicals. Journal of the American Chemical Society 94 (1), 47-57.

Kapoor, S. and Varshney, L. (1997) Redox Reactions of Chloramphenicol and Some Aryl Peroxyl Radicals in Aqueous Solutions: A Pulse Radiolytic Study. The Journal of Physical Chemistry A 101 (42), 7778-7782.

Lutze, H.V., Bircher, S., Rapp, I., Kerlin, N., Bakkour, R., Geisler, M., et al. (2015) Degradation of Chlorotriazine Pesticides by Sulfate Radicals and the Influence of Organic Matter. Environmental Science & Technology 49 (3), 1673-1680.

Mitchell, S.M., Ahmad, M., Teel, A.L. and Watts, R.J. (2014) Degradation of Perfluorooctanoic Acid by Reactive Species Generated through Catalyzed H2O2 Propagation Reactions. Environmental Science & Technology Letters 1 (1), 117-121.

Nihemaiti, M., Miklos, D.B., Hübner, U., Linden, K.G., Drewes, J.E. and Croué, J.-P. (2018) Removal of trace organic chemicals in wastewater effluent by UV/H2O2 and UV/PDS. Water Research 145, 487-497.

NIST (2020) The Radiation Chemistry Data Center of the Notre Dame Radiation Laboratory (ndrlRCDC) Kinetics Database.

Qian, Y., Guo, X., Zhang, Y., Peng, Y., Sun, P., Huang, C.-H., et al. (2016) Perfluorooctanoic Acid Degradation Using UV–Persulfate Process: Modeling of the Degradation and Chlorate Formation. Environmental Science & Technology 50 (2), 772-781.

Real, F.J., Benitez, F.J., Acero, J.L., Sagasti, J.J.P. and Casas, F. (2009) Kinetics of the Chemical Oxidation of the Pharmaceuticals Primidone, Ketoprofen, and Diatrizoate in Ultrapure and Natural Waters. Industrial & Engineering Chemistry Research 48 (7), 3380-3388.

Wei, Z., Villamena, F.A. and Weavers, L.K. (2017) Kinetics and Mechanism of Ultrasonic Activation of Persulfate: An in Situ EPR Spin Trapping Study. Environmental Science & Technology 51 (6), 3410-3417.
Yang, Y., Pignatello, J.J., Ma, J. and Mitch, W.A. (2014) Comparison of Halide Impacts on the Efficiency of Contaminant Degradation by Sulfate and Hydroxyl Radical-Based Advanced Oxidation Processes (AOPs). Environmental Science & Technology 48 (4), 2344-2351.
Zalibera, M., Rapta, P., Staško, A., Brindzová, L. and Brezová, V. (2009) Thermal generation of stable spin trap adducts with super-hyperfine structure in their EPR spectra: An alternative EPR spin trapping assay for radical scavenging capacity determination in dimethylsulphoxide. Free Radical Research 43 (5), 457-469.
Zhang, R., Yang, Y., Huang, C.-H., Zhao, L. and Sun, P. (2016) Kinetics and modeling of sulfonamide antibiotic degradation in wastewater and human urine by UV/H2O2 and UV/PDS. Water Research 103, 283-292.
Zhou, K., Wang, Z., Wang, X., Jiao, G., Li, Y., Sun, S.-P., et al. (2020) Degradation of emerging pharmaceutical micropollutants in municipal secondary effluents by low-pressure UVC-activated HSO5− and S2O82− AOPs. Chemical Engineering Journal 393, 124712.